IEEE Access
Multidisciplinary | Rapid Review | Open Access Journal

Received December 15, 2016, accepted January 3, 2017, date of publication February 6, 2017, date of current version March 13, 2017.

Digital Object Identifier 10.1109/ACCESS.2017.2653798

Fast and Efficient Radio Resource Allocation in Dynamic Ultra-Dense Heterogeneous Networks

CHONGYU NIU[1], YIBING LI[1], (Member, IEEE), ROSE QINGYANG HU[2], (Senior Member, IEEE), AND FANG YE[1], (Member, IEEE)

[1]Department of Information and Communication Engineering, Harbin Engineering University, Harbin 150001, China
[2]Department of Electrical and Computer Engineering, Utah State University, Logan, UT 84322, USA

Corresponding author: Y. Li (liyibing@hrbeu.edu.cn)

This work was supported in part by the National Natural Science Foundation of China under Grant 51509049, in part by the National Key Research and Development Program under Grant 2016YFF0102806, in part by the Fundamental Research Funds for the Central Universities of China under Grant GK2080260140, and in part by the National Science Foundation under Grant ECCS-1308006 and Grant EARS-1547312.

ABSTRACT Ultra-dense network (UDN) is considered as a promising technology in 5G wireless networks. In an UDN network, dynamic traffic patterns can lead to a high computational complexity and an excessive communications overhead with traditional resource allocation schemes. In this paper, a new resource allocation scheme presenting a low computational overhead and a low subband handoff rate in a dynamic ultra-dense heterogeneous network is presented. The scheme first defines a new interference estimation method that constructs network interference state map, based on which a radio resource allocation scheme is proposed. The resource allocation problem is a MAX-K cut problem and can be solved through a graph-theoretical approach. System level simulations reveal that the proposed scheme decreases the subband handoff rate by 30% with less than 3.2% network throughput degradation.

INDEX TERMS Ultra-dense HetNets, graph theory, femtocell, MAX-K cut.

I. INTRODUCTION

The demand for ubiquitous availability of reliable and high data rate mobile services is ever increasing. Mobile data traffic demand has been predicted to have a 1000-fold increase in the next 20 years [1], [2]. To meet the explosive capacity increase of mobile communication systems, Ultra-dense Networking (UDN) has been widely considered as a promising technology [3]. In addition, studies predict that more than 50% of voice calls and more than 70% of data traffic in the future wireless networks originated from indoors [4]. Thus, indoor femtocells (FCs) will play a significant role in the 5G network access, especially for low velocity or stationary users [5]. Ultra-dense deployed FCs overlaid with traditional macrocells (MCs) lead to a more advanced network, namely, Ultra-Dense Heterogeneous Network (UDHN).

With the enormous growth of mobile devices capacity and cloud computing, the latency of the communication, reliability of the services, and pervasive availability of the networks are among the most important performance metrics when deploying 5G UDHNs. According to the METIS project, there are mainly five features of 5G communication systems: 1) amazingly fast, 2) great service in a crowd, 3) ubiquitous things communicating, 4) best experience follows you, and 5) super real-time and reliable connections [6]. In UDHNs, there are a number of technical challenges [7], among which one of the most important challenges is how to efficiently allocate and utilize subband resources to improve the spectrum efficiency and mitigate interference. Furthermore, in a dynamic UDHN, subband resource allocation should be rather stable and any subband handoff should be swift.

There have been extensive ongoing researches on subband resource allocation [8]–[10], which are mainly classified into centralized approaches and decentralized approaches. However, most of the existing schemes used in the traditional heterogeneous networks(HetNets) will not be suitable in the UDHN mainly due to two reasons. i) Existing decentralized approaches converge slowly due to a large number of nodes in the UDHN and thus real-time and reliable requirements of UDHN are difficult to achieve. ii) Traditional centralized approaches can achieve optimal/near-optimal performance while the huge computational overhead stays as a concern. Thus an efficient resource allocation scheme that provides rapid and stable resource allocation decisions for a dynamic UDHN is urgently needed.

Lately extensive work have been done on dynamic interference mitigation in UDHNs. In [11]–[17], the authors worked on the resource allocation problem using a clustering based graph scheme. In [11], clustering based resource allocation scheme was investigated in a densely deployed femtocell network. In that paper, the resource allocation problem is formulated as a mixed integer non-linear program, and the proposed scheme can achieve near optimal performance with a reduced computational complexity. Anjum *et al.* [12] considered the real time interference and traffic characteristics jointly in heavily overlapped femtocells by using a clustering scheme. In [13], a suboptimal subband assignment and interference management algorithm was designed based on an adaptive graph coloring approach and fractional frequency reuse scheme. [11]–[13] can achieve a good performance in controlling co-tier interference and cross-tier interference. However they are less effective in handling dynamic network conditions in an UDHN. In [14]–[17], dynamic network conditions were investigated. In [14], a dynamic graph based scheme was proposed to coordinate dynamic interference. In that scheme, a two tier clustering scheme is used to divide femtocells and UEs into several small groups. While the proposed scheme can achieve a near optimal performance, its potential high communication overhead is not evaluated. In [15], a multi-cluster based dynamic subband assignment method is discussed in UDNs. The scheme divides the entire spectrum into two groups, namely dynamic group and static group. Static UEs can get a stable transmit experience. But the spectrum partition actually lowers down the spectral efficiency. Further, the scheme presents a high computational complexity. Yoon *et al.* [16] proposed an interference weight calculation algorithm to reduce the computational complexity of the dynamic cell clustering scheme. The computational complexity can be reduced to half compared to the traditional clustering based scheme, but the feasibility of this algorithm in dynamic UDHNs is not discussed. In [17], an interference-separation clustering based scheme is used to lower down the communication overhead and computational complexity in dynamic UDHNs. In this scheme, massive small cells are divided into different small groups with different priorities to reduce the complexity. This scheme can achieve a real time resource allocation, while the spectral efficiency is low.

Subband handoff between different time slots has all been ignored in the above papers. Unnecessary subband handoff leads to a high latency, a high computation overhead, and a low reliability of the services. To tackle this problem, in this paper a new fast subband allocation scheme with low subband handoff rate is proposed based on the graph clustering theory. Further, a more flexible UFR approach is used to offer a higher spectral efficiency in this paper. The proposed scheme first presents the system model and proposes a potential interference estimation method between different users in HetNets, including intra-tier and inter-tier interference estimation. A network Interference State Map (ISM) is constructed to compare the network state information between different subband allocation time slots (TSs). Afterwards, an advanced cluster-based subband allocation algorithm in a universal spectrum reuse scheme is discussed and a fast subband allocation scheme (FAS) based on the ISM and subband allocation algorithm is presented.

The main contributions of this paper are summarized in the following. First, a new fast subband allocation scheme with a low subband handoff rate is developed. Second, a new interference evaluation model in two-tier ultra-dense deployed heterogeneous networks is defined. Third, a new ISM model is proposed to represent the interference in HetNets.

The remainder of this paper is organized as follows. The system model is shown in Section II. In Section III, the fast subband allocation scheme is elaborated. Section IV evaluates the performance of the proposed scheme via simulations. Section V draws the conclusion of the paper.

II. SYSTEM MODEL AND PROBLEM FORMULATION

A. SYSTEM MODEL

In a two-tier UHDN, an MBS with a coverage radius R_M is located at the center with a number of FBSs densely deployed within the coverage of that MBS. Two different UEs are considered, namely MUEs served by the MBS and FUEs served by FBSs. Both MUEs and FUEs are uniformly distributed with respective densities as λ_m and λ_f [18]. FBSs constitute the femto-tier and the coverage area of each FBS is a circular region with a radius of R_f. In an UDHN, different FBSs can have overlapped coverage areas due to the high density of FBSs. So the actual service area of FBSs induces a Voronoi tessellation [19], as shown in Fig. 1.

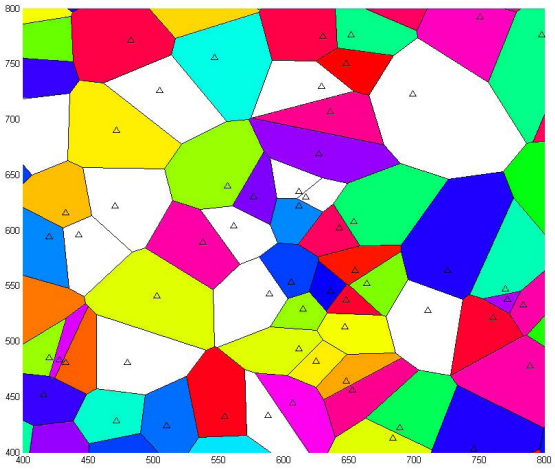

FIGURE 1. The Voronoi Femtocell topology (Δ stands for an FBS).

In the considered UDN, time domain consists of time slots and the resource allocation decision is made every time slot. Further, in each time slot t, $n_{(m,t)}$ MUEs and $n_{(f,t)}$ FUEs can join, leave or change their locations in the network. Each cell, either an MC or a FC, constitutes an independent agent that performs autonomous radio resource allocation decisions with the objective of improving UE signal to interference plus noise ratio (SINR) while guaranteeing UE quality of

service (QoS). All the system configuration information is accessible at the MBS. These information can include geographic locations of MUEs, FBSs and FUEs, the channel fading parameters, and dynamic system information.

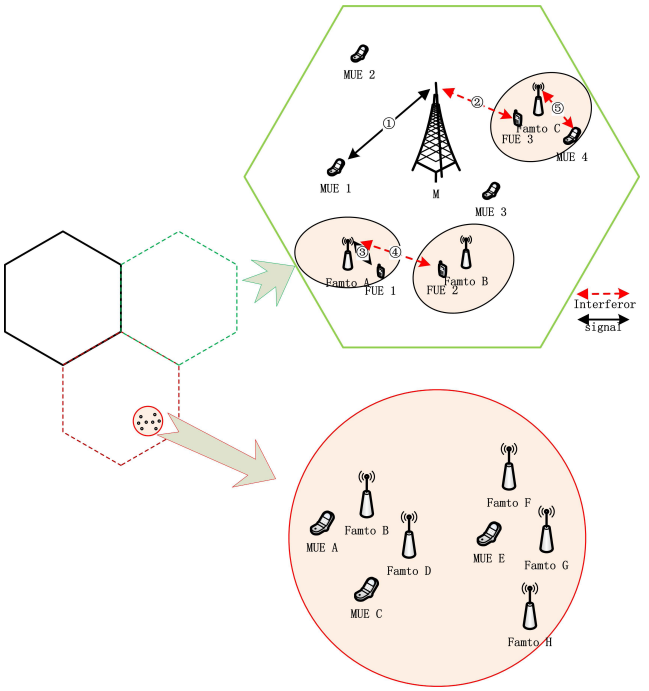

FIGURE 2. Proposed dense framework for Subband assignment.

As shown in the green marked part in Fig. 2, wireless links and their respective received powers in this UHDN can be classified into five types by following the same definitions in [20]:

(1) Outdoor link from MBS to MUE m

$$P_m^{k,t} = P_{B,m}^{k,t} h_{B,m}^{k,t} G_{B,m}^{k,t}. \tag{1}$$

(2) Outdoor-to-Indoor link from MBS to FUE j_f

$$I_{B,j_f}^{k,t} = \sum_{m \in \boldsymbol{M}} s_m^{k,t} P_{B,m}^{k,t} h_{B,j_f}^{k,t} G_{B,j_f}^{k,t}. \tag{2}$$

(3) Indoor link from FBS f to its serving FUE j_f

$$P_{j_f}^{k,t} = P_{f,j_f}^{k,t} h_{f,j_f}^{k,t} G_{f,j_f}^{k,t}. \tag{3}$$

(4) Indoor-to-indoor link from FBSs in the different FCs to FUE j_f

$$I_{\boldsymbol{F^*},j_f}^{k,t} = \sum_{f^* \in \boldsymbol{F^*}} \sum_{j_{f^*} \in \boldsymbol{J_{f^*}}} s_{j_{f^*}}^{k,t} P_{f^*,j_{f^*}}^{k,t} h_{f^*,j_f}^{k,t} G_{f^*,j_f}^{k,t}. \tag{4}$$

(5) Indoor-to-Outdoor link from FBS to MUE m

$$I_{\boldsymbol{F},m}^{k,t} = \sum_{f \in \boldsymbol{F}} \sum_{j_f \in \boldsymbol{J_f}} s_{j_f}^{k,t} P_{f,j_f}^{k,t} h_{f,m}^{k,t} G_{f,m}^{k,t}. \tag{5}$$

$\boldsymbol{K} = \{k|k = 1, 2, ldots, K\}$ stands for the set of total subbands; $\boldsymbol{M} = \{m|m = 1, 2, ldots, M\}$ stands for the set of MUEs located in the coverage area of the MBS; $\boldsymbol{F} = \{f|f = 1, 2, ldots, F\}$ stands for the set of FBSs located in the coverage of MBS; $\boldsymbol{F^*} : \{f^* \in \boldsymbol{F^*}\}$ stands for the set of FBSs located in the coverage of MBS but exluding FBS f; $\boldsymbol{J_f} : \{j_f \in \boldsymbol{J_f}\}$ stands for the set of FUEs served by FBS f; $\boldsymbol{J_F} : \{\boldsymbol{J_f} \in \boldsymbol{J_F}\}$ stands for the set of FUEs in the coverage of the MBS; B stands for the MBS; $P_{B,m}^{k,t}$ ($P_{f,j_f}^{k,t}$) stands for the transmit power from MBS (FBS f) to MUE m (FUE j_f) on subband k in time slot t; $h_{B,m}^{k,t}$ ($h_{f,j_f}^{k,t}$) denotes the channel gain from MBS (FBS f) to MUE m (FUE j_f) on subband k in time slot $t$and follows an exponential distribution; $G_{B,m}^{k,t}$ ($G_{f,j_f}^{k,t}$) denotes the path loss from MBS (FBS f) to MUE m (FUE j_f) on subband k in time slot t. $s_m^{k,t}$ is the subband allocation indicator, i.e., $s_m^{k,t} = 1$ if subband k is assigned to UE m in time slot t , while $s_m^{k,t} = 0$ otherwise. We assume the same K channels are used in all the cells, including one MBS and N_F FBSs.

$SINR_m^{k,t}$ represents the SINR for downlink transmission from MBS to MUE m on subband k in time slot t and is expressed as:

$$SINR_m^{k,t} = \frac{P_m^{k,t}}{I_{\boldsymbol{F},m}^{k,t} + N_0}. \tag{6}$$

The SINR for downlink transmission from FBS f to FUE j_f on subband k in time slot t is given by:

$$SINR_{j_f}^{k,t} = \frac{P_{j_f}^{k,t}}{I_{B,j_f}^{k,t} + I_{\boldsymbol{F^*},j_f}^{k,t} + N_0}. \tag{7}$$

$I_{\boldsymbol{F},m}^{k,t}$ represents the interference from all co-channel FBSs to MBS on channel k in time slot t; $I_{B,j_f}^{k,t}$ represents co-channel interference from MBS to FBS j_f on channel k in time slot t; $I_{\boldsymbol{F^*},j_f}^{k,t}$ represents co-channel interference from all other FBSs to FBS j_f on channel k in time slot t; N_0 stands for the noise level.

B. PROBLEM FORMULATION

FUEs in the serving area of each FBS are allocated orthogonal resources from that FBS. Radio resources are allocated in the unit of subband and each UE is assumed to be assigned an equal number of subbands. Without loss of generality, it is assumed that one subband is allocated to each UE. The FAS scheme aims to construct a fast subband allocation while minimizes unnecessary subband handoff among UEs. UEs that stay in the same condition (including location, active/idle state) in two consecutive time slots are defined as static users (U^S), which include static macro UEs (U_M^S) and static femto UEs (U_F^S). Also, UEs that join, leave or change their locations in two consecutive time slots are defined as dynamic UEs (U^D), including dynamic macro UEs (U_M^D) and dynamic femto UEs (U_F^D). To save energy, FBSs serving no FUE are turned off and they will only receive system control information. If one off-FBS detects that there is any UE in its serving area, this off-FBS will be turned on. The turned-off FBSs are shown as white colored areas in Fig. 1. Only FBSs with active

FUEs are allocated subbands. So the total number of FBSs keep the same but the number of active FBSs may change from time to time.

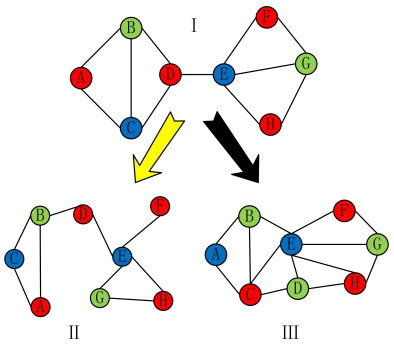

FIGURE 3. Network interference topology variation due to UE mobility.

Due to dynamics in the network, within two consecutive time slots, the network interference topology can change. Fig. 3.I is the network interference topology of red marked area as shown in Fig. 2, where circles stand for UEs, solid lines between different circles stand for co-channel interference, and different colors stand for different subbands. The corresponding interference matrix can be expressed as:

$$I_I = \begin{bmatrix} i_{AA} & i_{AB} & \cdots & i_{AH} \\ i_{BA} & \ddots & & \vdots \\ \vdots & & \ddots & \vdots \\ i_{HA} & \cdots & \cdots & i_{HH} \end{bmatrix} = \begin{bmatrix} 1 & 1 & 1 & 0 & 0 & 0 & 0 & 0 \\ 1 & 1 & 1 & 1 & 0 & 0 & 0 & 0 \\ 1 & 1 & 1 & 1 & 0 & 0 & 0 & 0 \\ 0 & 1 & 1 & 1 & 1 & 0 & 0 & 0 \\ 0 & 0 & 0 & 1 & 1 & 1 & 1 & 1 \\ 0 & 0 & 0 & 0 & 1 & 1 & 1 & 0 \\ 0 & 0 & 0 & 0 & 1 & 1 & 1 & 1 \\ 0 & 0 & 0 & 0 & 1 & 0 & 1 & 1 \end{bmatrix}. \quad (8)$$

As UEs move, the network interference topology may become Fig. 3.II and Fig. 3.III. The corresponding interference matrix of II is:

$$I_{II} = \begin{bmatrix} 1 & 1 & 1 & 0 & 0 & 0 & 0 & 0 \\ 1 & 1 & 1 & 1 & 0 & 0 & 0 & 0 \\ 1 & 1 & 1 & 0 & 0 & 0 & 0 & 0 \\ 0 & 1 & 0 & 1 & 1 & 0 & 0 & 0 \\ 0 & 0 & 0 & 1 & 1 & 1 & 1 & 1 \\ 0 & 0 & 0 & 0 & 1 & 1 & 0 & 0 \\ 0 & 0 & 0 & 0 & 1 & 0 & 1 & 1 \\ 0 & 0 & 0 & 0 & 1 & 0 & 1 & 1 \end{bmatrix}. \quad (9)$$

Comparing interference matrices (8) and (9), one can see that even though UEs A, C, D, and G change their respective locations, the interference relationship between different UEs still keep quite the same. Thus there is no need to change the original subband allocations among UEs. In a different scenario, as shown in Fig. 3.III, even though only UEs D and E change their locations, the entire network interference relationship changes and the corresponding new interference matrix of III becomes:

$$I_{III} = \begin{bmatrix} 1 & 1 & 1 & 0 & 0 & 0 & 0 & 0 \\ 1 & 1 & 1 & 0 & 1 & 0 & 0 & 0 \\ 1 & 1 & 1 & 1 & 1 & 0 & 0 & 0 \\ 0 & 0 & 1 & 1 & 1 & 0 & 0 & 1 \\ 0 & 1 & 1 & 1 & 1 & 1 & 1 & 1 \\ 0 & 0 & 0 & 0 & 1 & 1 & 1 & 0 \\ 0 & 0 & 0 & 0 & 1 & 1 & 1 & 1 \\ 0 & 0 & 0 & 1 & 1 & 0 & 1 & 1 \end{bmatrix}. \quad (10)$$

From matrices (8) and (10), the network subbands need to be re-allocated and we call this reallocation as subband handoff. The condition that triggers subband handoff is critical in the FAS scheme. As such, subband handoff indicator (SSI) is defined to represent the subband handoff. We have $SSI_u^t = 0$ when the following conditions are met.

$$\begin{cases} s_u^{k,t} = s_u^{k',t-1}; \\ s_u^{k,t} = 1, \qquad \forall k, k' \in \boldsymbol{K}, u \in \boldsymbol{U}; \\ k = k'. \end{cases} \quad (11)$$

Otherwise, $SSI_u^t = 1$. $s_u^{k,t}(s_u^{k',t-1})$ is the subband allocation indicator. $\boldsymbol{U} = \boldsymbol{M} \cup \boldsymbol{J_F}$ is the set of all UEs in the coverage area of MBS.

The objective of the proposed scheme is to minimize the subband handoff frequency (SHF). The optimization problem is formulated as:

$$\min\left(\frac{\sum_{t\in\boldsymbol{T}} SSI_u^t}{|\boldsymbol{T}|}\right), \forall u \in \boldsymbol{U}, \quad (12)$$

where $\boldsymbol{T}$ is the set of time slots.

III. PROPOSED SOLUTION

A. INTERFERENCE ESTIMATION

In the FAS scheme, the subband resource allocation can be decided based on the interference matrix. In UDHNs, network interference topology can be much more complicated than what is shown in Fig. 3.

To further evaluate the total potential influence a UE causes to the entire network when it uses a specific subband, Accumulate Regional Average Interference Strength (AAS) is defined. We use the coverage area as the evaluating area of one FBS. The calculation method of AAS varies between MUE and FUE. This paper follows the interference evaluation method defined in [21] with some changes.

1) FUEs AAS

The total potential influence that a FUE causes to the entire network in an UDN is defined in the same way in [21], which is summarized in the following.

$$I_f^{AAS} = I_f^{SAI} = \sum_{f^*\in\boldsymbol{F^*}} \frac{1}{1 + 2d_{f^*,f}^2 \psi_{f^*}} + \sum_{m\in\boldsymbol{M}} \frac{P_f {d_{m,B}}^2}{P_B {d_{m,f}}^2}. \quad (13)$$

2) MUEs AAS

When an MUE uses a specific subband, the potential influence it causes to other MUEs needs to be evaluated. The AAS from an MUE to other UEs is the AAS from MBS to all the other MUEs and FBSs in the coverage of this MBS. Here these two interference scenarios are discussed separately.

- AAS for Intra-tier Interference

$$I^{AAS}_{(m^*,m)} = \sum_{\substack{m^*,m\in\boldsymbol{M}\\ m^*\neq m}} \frac{1}{SINR_{m^*}} = \sum_{\substack{m^*,m\in\boldsymbol{M}\\ m^*\neq m}} \frac{1}{\frac{P_B d_{m^*,B}^{-\frac{\alpha}{2}}}{P_{m,B} d_{m^*,B}^{-\frac{\alpha}{2}} \lambda_{m^*,m}}}. \quad (14)$$

In this paper, we assume the MBS equally divides its transmit power among all subbands. So we have

$$I^{AAS}_{(m^*,m)} = \sum_{\substack{m^*,m\in\boldsymbol{M}\\ m^*\neq m}} \lambda_{m^*,m}, \quad (15)$$

subject to:

$$\begin{cases} \lambda_{m^*,m} = 1, & \boldsymbol{\Theta_m} = \boldsymbol{\Theta_{m^*}}; \\ \boldsymbol{\varpi}^{-1}, & \boldsymbol{\Theta_m} \neq \boldsymbol{\Theta_{m^*}}. \end{cases} \quad (16)$$

$\boldsymbol{\varpi}$ stands for the antenna back loss; $\boldsymbol{\Theta_m}$ stands for the sector label of UE m.

- AAS for Inter-cell Interference
The total potential influence that a MUE makes to the FBSs in an UDN is also defined in the same way in [21]), where the AAS for MUE m to FBSs is expressed as

$$I_{(\boldsymbol{F},m,\boldsymbol{A_F})} = I_f^{SAI} = \sum_{f\in\boldsymbol{F}} \frac{P_B}{P_f\left(1+2d_{f,B}^2\psi_f\right)}. \quad (17)$$

$d_{f,B}$ stands for the distance between FBS f and MBS.

In summary, the AAS for MUE m, including both intra-tier and inter-tier AAS, can be expressed as:

$$I_m^{AAS} = \sum_{\substack{m^*,m\in\boldsymbol{M}\\ m^*\neq m}} \lambda_{m^*,m} + \sum_{f\in\boldsymbol{F}} \frac{P_B}{P_f\left(1+2d_{f,B}^2\psi_f\right)}. \quad (18)$$

B. NETWORK INTERFERENCE STATE MAP

In this section we discuss the network interference state map (ISM) construction process. The ISM covers an area of $2*R_M*\sqrt{3}R_M$ with $\Psi*0.866*\Psi$ pixels, where the length of one pixel ψ is the minimum distance between two different users, $\Psi = \frac{2R_M}{\psi}$. The MBS locates at the center of the ISM with a coordinate $(0, 0)$. The coverage area of the MBS is divided into three sectors, sector.0, sector.1 and sector.3. We set the value of the pixels located outside the hexagonal MBS coverage area as 0. The interference map includes two layers, MUE layer and FBS layer, which are discussed separately in the following.

1) ISM PIXEL WEIGHT FOR MUE LAYER

We first calculate the average interference weight $h_m(i, j)$ on ISM pixel with coordinate $(i,\ j)$. Without loss of generality, sector.0 is used as the tagged sector for study.

$$I_{\boldsymbol{M}}^{AAS} = \sum_{m\in\boldsymbol{M_{S_0}}} I_m^{AAS}. \quad (19)$$

$$h_m(i,j) = \frac{I_{\boldsymbol{M}}^{AAS}}{3\,(2n-1)\,n_k \sum_{n=1}^{\Psi}\frac{1}{2n-1}}. \quad (20)$$

$\boldsymbol{M_{S_0}}$ stands for the set of MUEs located at sector 0; n_k is the total number of pixels whose distance d from the center point satisfies $(n-1)\,\psi < d \leq n\psi$ and $d^2 = i^2 + j^2$. The calculation of h_n is detailed in Appendix. A. Thus ISM of MUE layer can be constructed in Fig. 4. The ISM of MBS tier changes from sector to sector. Within each sector, as long as the number and locations of MUEs keep unchanged, the ISM for that sector stays the same.

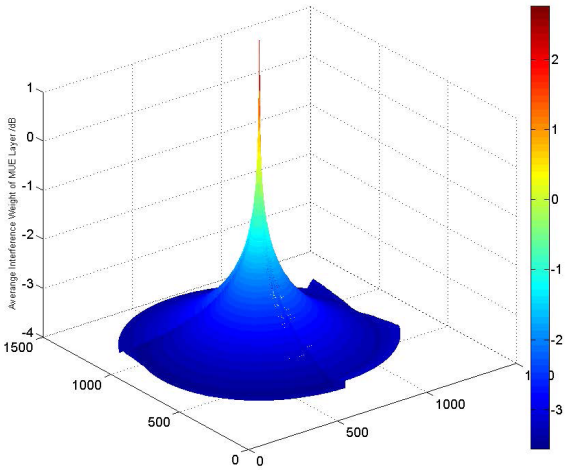

FIGURE 4. ISM for MUE layer.

2) ISM PIXEL WEIGHT FOR FBS LAYER

In an UDHN, the locations of FBSs in reality do not change quite often. However, the active/idle state of each FBS can vary from time to time. As each FBS has a Voronoi serving area, the average interference weight $h_f(i,\ j)$ contributed by FBS f to the ISM pixel in the coverage area of FBS f is:

$$h_f(i,j) = \frac{t_f I_f^{AAS}}{n_f}, \quad (21)$$

$$n_f = \frac{S_f}{\psi^2}. \quad (22)$$

t_f is the FBS activation state indicator, i.e. $t_f = 1$ if FBS f is active (i.e., there are active FUEs in the serving area of FBS f), while $t_f = 0$ otherwise. n_f is the total number of pixels in the coverage area of FBS f. S_f is the total coverage area of FBS f. So the ISM of FBS layer can be constructed in Fig. 5.

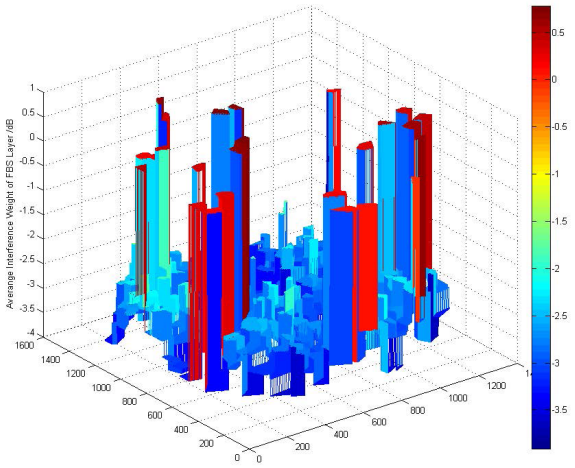

FIGURE 5. ISM for FBS layer.

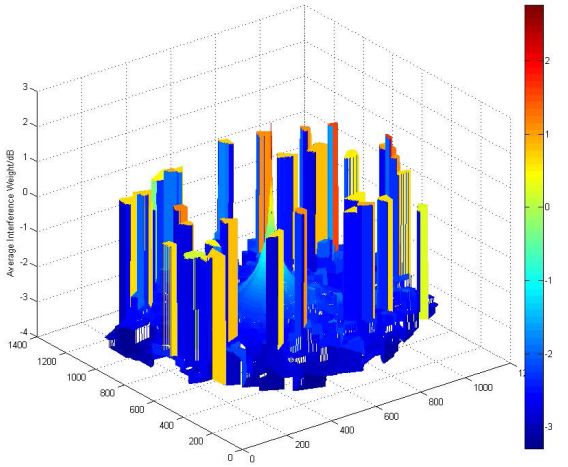

FIGURE 6. ISM.

When combining the ISM maps from MBS and FBS layers one can get the ISM of the entire network, as shown in Fig. 6.

$$ISM(i,j) = h_m(i,j) + h_f(i,j). \tag{23}$$

C. ISM SIMILARITY CALCULATION

In the FAS scheme, similarity among ISMs in two consecutive time slots needs to be evaluated. Structural Similarity (SSIM) has been proposed in [22] and [23] for that purpose. Assume SSIM is calculated between t_0 and t_1.

$$\begin{aligned} &SSIM(ISM^{t_0}, ISM^{t_1}) \\ &\quad = SSIM_{(0,1)} \\ &\quad = S_{(0,1)} \\ &\quad = l(t_0,t_1)\cdot c(t_0,t_1)\cdot s(t_0,t_1), \end{aligned} \tag{24}$$

$$l(t_0,t_1) = \frac{2\mu_{t_0}\mu_{t_1} + C_1}{\mu_{t_0}^2 + \mu_{t_1}^2 + C_1}, \tag{25}$$

$$c(t_0,t_1) = \frac{2\sigma_{t_0}\sigma_{t_1} + C_2}{\sigma_{t_0}^2 + \sigma_{t_1}^2 + C_2}, \tag{26}$$

$$s(t_0,t_1) = \frac{\sigma_{t_0t_1} + C_3}{\sigma_{t_0}\sigma_{t_1} + C_3}, \tag{27}$$

$$\mu_{t_0} = \frac{1}{H*W}\sum_{i=1}^{H}\sum_{j=1}^{W} ISM_{(i,j)}^{t_0}, \tag{28}$$

$$\mu_{t_1} = \frac{1}{H*W}\sum_{i=1}^{H}\sum_{j=1}^{W} ISM_{(i,j)}^{t_1}, \tag{29}$$

$$\sigma_{t_0}^2 = \frac{1}{H*W-1}\sum_{i=1}^{H}\sum_{j=1}^{W}\left(ISM_{(i,j)}^{t_0} - \mu_{t_0}\right)^2, \tag{30}$$

$$\sigma_{t_1}^2 = \frac{1}{H*W-1}\sum_{i=1}^{H}\sum_{j=1}^{W}\left(ISM_{(i,j)}^{t_1} - \mu_{t_1}\right)^2, \tag{31}$$

$$\begin{aligned} \sigma_{t_0t_1} = &\frac{1}{H*W-1}\sum_{i=1}^{H}\sum_{j=1}^{W}\left(ISM_{(i,j)}^{t_0} - \mu_{t_0}\right) \\ &\times\left(ISM_{(i,j)}^{t_1} - \mu_{t_1}\right), \end{aligned} \tag{32}$$

subject to:

$$\begin{cases} C_1 = (K_1 \times L)^2, \\ C_2 = (K_2 \times L)^2, \\ C_3 = \dfrac{C_2}{2}, \\ K_1 = 0.01, \\ k_2 = 0.03, \\ L = ISM_{max}. \end{cases} \tag{33}$$

$ISM_{(i,j)}^{t_0}$ stands for the interference weight of pixel (i,j) in the ISM at t_0; H stands for the height of the ISM, where $H = \Psi$; W stands for the width of the ISM, where $W = 0.866\Psi$; ISM_{max} stands for the biggest interference weight on one pixel. Normally ISM_{max} is attained in a highly dense situation, where the distance between two nearest MUEs is defined as $d_{min,m}$ and the distance between two nearest FBSs is $R_{min,f}$. It is assumed that $d_{min,m} = R_{min,f}$. The calculation of ISM_{max} is provided in Appendix. B.

D. ADVANCED CLUSTER-BASED SUBBAND ALLOCATION ALGORITHM(ASA)

The cluster-based subband allocation scheme has been discussed in [21]. Based on the T-HCDA algorithm proposed in [21], in this paper we propose an advanced subband allocation algorithm that can better address dynamic conditions in an UDN. In this scheme, the MBS makes the allocation decision, including the interference graph $G(V,E)$ construction and subband resource allocation. The vertex set V includes all the FBSs and all the MUEs, edge set E stands for the interference relationship between different vertexes. KG is the weight matrix to characterize the potential interference between two vertexes. The calculation of KG is the same as in [21].

Upon the construction of interference graph, the subband allocation problem becomes a cluster based graph MAX-K cut problem, in which UEs in the same cluster can share

the same subband. Assume that the number of subbands is $K = |\boldsymbol{K}|$ and the weight between node i and node j is kg_{ij}. An advanced cluster-based subband allocation algorithm (ASA) is proposed to control the subband allocation process.

In the ASA algorithm, the nodes are partitioned into K disjoint sets $\boldsymbol{D} = \boldsymbol{D}_1 \cup \boldsymbol{D}_2 \cup ... \cup \boldsymbol{D}_K$ that maximize the weights between the disjoint sets in $G = (V, E)$. We first assign every node a certain interference weight label, where the weight label of every node is:

$$\boldsymbol{L_V} = \{l_v | l_v = I_v^{AAS}, v \in \boldsymbol{V}\}. \tag{34}$$

In the following process of ASA, there are two conditions:

- The initial cluster set $\boldsymbol{D}$ is empty.
  We name this condition as original subband allocation circulation (OSAC). OSAC consists of two steps. In Step one, we first choose K nodes with the smallest label as the cluster of K clusters. In Step two, the rest nodes are assigned to the clusters one by one by following an ascending label sequence. Only when the following constraints are satisfied can node v be assigned to cluster k:
  $$\begin{cases} \Delta KG_k \leq \Delta KG_a, & \forall a \in K; \\ \Delta KG_k = \sum_{u \in \boldsymbol{D}_k} kg_{vu}. \end{cases} \tag{35}$$
- The initial cluster set $\boldsymbol{D}$ is not empty.
  We name this condition as a halfway subband allocation circulation (HSAC). In the HSAC, the nodes that remain in the cluster set $\boldsymbol{D}$ will be assigned to the original cluster that they stay in the last subband allocation time slot. That means these nodes will not switch their subbands. After that, the rest nodes that are not in $\boldsymbol{D}$ are assigned to the clusters by following Step two of OSAC.

The pseudo-codes of the ASA algorithm are listed in Algorithm 1.

Algorithm 1 ASA Algorithms

Initialization: $\boldsymbol{F}$; $\boldsymbol{M}$;$\boldsymbol{K}$; $\boldsymbol{V} = \boldsymbol{F} \cup \boldsymbol{M}$; $KG = \left[kg_{ij}\right]_{N \times N}$, $N = |\boldsymbol{V}|$; $N_M = |\boldsymbol{M}|$, $N_F = |\boldsymbol{F}|$; $N_{J_f} = |\boldsymbol{J_f}|$, the number of FUEs served by FBS is f; $\boldsymbol{L_V}$ is the label matrix of every node; Ω_v is the degree of vertex v; $\boldsymbol{D_k}$ is the set of nodes in cluster k.

function Label Process
  Label every node v with l_v, where $l_v = I_v^{AAS}$.
end function
function Cluster Process
  if $\boldsymbol{D} = \emptyset$ **then**;
    From $\boldsymbol{L_V}$ $\downarrow$; $\forall v \in \boldsymbol{V}, k \in \boldsymbol{K}$;
    if cluster k is empty **then**
      $v \rightarrow \boldsymbol{D}_k$;
    else
      Calculate $\Delta KG_k = \sum_{u \in \boldsymbol{D}_k} kg_{vu}$;
      $k = \arg\min \Delta KG$;
      $v \rightarrow \boldsymbol{D}_k$;
    end if
  else
    $\boldsymbol{V'} = \{v | v \notin \boldsymbol{D}\}$;
    From $L_{V'}$ $\downarrow$; $\forall v' \in \boldsymbol{V'}, k \in \boldsymbol{K}$;
    if cluster k is empty **then**
      $v' \rightarrow \boldsymbol{D}_k$;
    else
      Calculate $\Delta KG_k = \sum_{u \in \boldsymbol{D}_k} kg_{v'u}$;
      $k = \arg\min \Delta KG$;
      $v' \rightarrow \boldsymbol{D}_k$;
    end if
  end if
end function

E. FAST SUBBAND ALLOCATION SCHEME

We further propose a new Fast Subband Allocation (FAS) scheme. It is assumed that the MBS will make the resource allocation decisions and the MBS stores all the allocation results. At each time slot, the FAS scheme consists of three steps:

1) STEP 1: ISM CONSTRUCTION

In this step the MBS first constructs the ISM, defined as ISM^1, of the entire network, according to the method in subsection.B. The ISM constructed in the previous time slot is defined as ISM^0.

2) STEP 2: ISM MATCHING

If $ISM^0 = \emptyset$, go to Step 3 directly. Otherwise calculate SSIM $S_{(0,1)}$ of ISM^1 and ISM^0. Compare the SSIM value with the ISM Similarity Factor threshold S_{th}.

- If $S_{(0,1)} \geq S_{th}$, $\boldsymbol{D_0}$ is updated to $\boldsymbol{D}$ by keeping static UEs in $\boldsymbol{D_0}$ and remove dynamic UEs from $\boldsymbol{D_0}$.
- If $S_{(0,1)} < S_{th}$, $\boldsymbol{D}$ is set to empty.

3) STEP 3: SUBBAND ALLOCATION

MBS assigns each UE to a cluster according to the ASA algorithm and cluster set $\boldsymbol{D_1}$ is formed. The corresponding variables are updated in the following.

- If $S_{(0,1)} \geq S_{th}$, both $\boldsymbol{D_0}$ and $\boldsymbol{ISM^0}$ remain unchanged.
- If $S_{(0,1)} < S_{th}$, update $\boldsymbol{D_0}$ and $\boldsymbol{ISM^0}$ with $\boldsymbol{D_1}$ and $\boldsymbol{ISM^1}$ respectively.

The corresponding algorithm flowchart of FAS scheme is presented in Fig.7. The computational complexity of this scheme consists of three parts. The first part comes from the potential interference estimation, which has a computation complexity $O((N^D)^2)$, $N^D = |\boldsymbol{U_M^D} \cup \boldsymbol{U_F^D}|$. The second part comes from ISM construction, which has a computational complexity $O(\Psi^2)$ and is only a function of the network size. The third part comes from the subband allocation, which has a complexity of $O(\frac{(N+N-N^D)(N-N+N^D)}{2}) \approx O((N^D)^2)$. Thus the total computational complexity of the FAS scheme is $O((N^D)^2)$.

Since the cluster-based resource allocation is a roll polling algorithm, in every polling circle, one UE is allocated to a cluster. After N polling circles, the algorithm reaches convergence. In this paper, we propose the FSA algorithm,

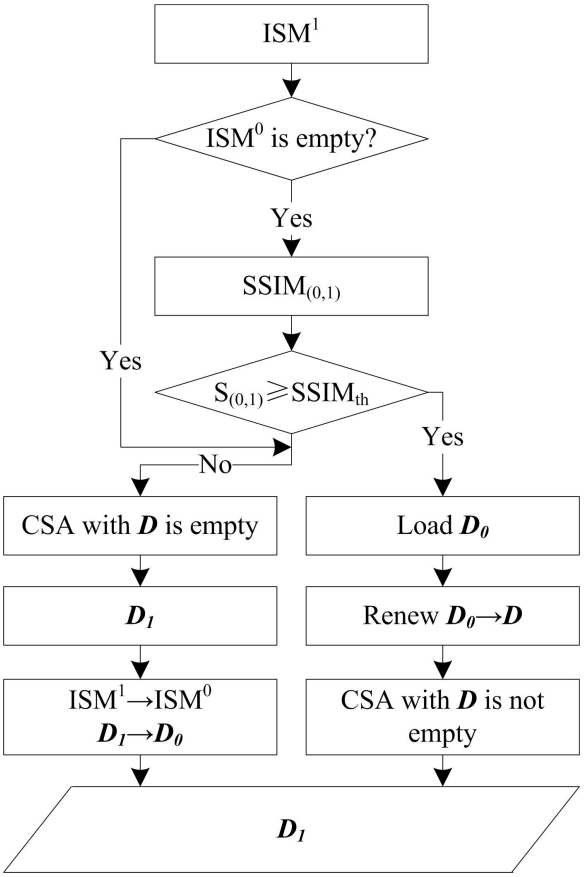

FIGURE 7. FAS scheme flowchart.

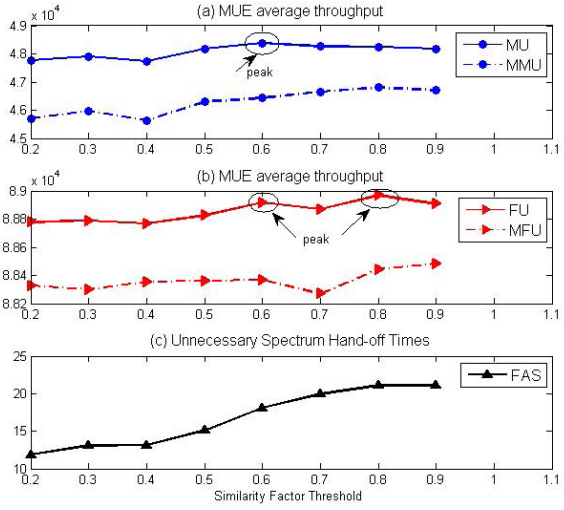

FIGURE 8. Average UE throughput and Subband Handoff time (NHT) with different similarity factor threshold S_{th}.

in which there are two kinds of polling process. In the common resource allocation polling process, N UEs join the polling process. After N polling circles, the algorithm for sure reaches convergence. In the fast resource allocation polling process, N^D dynamic UEs join the polling process. After N^D polling circles, the algorithm for sure reaches convergence.

TABLE 1. Simulation Parameters

Parameters	Macrocell	Femtocell
System Bandwith	20MHz	20MHz
Subcarrier spacing	180kHz	180kHz
Cell Size	ISD = 500m	Radius = 20m
Cell-center Size	350m	–
Sectors	3	1
Transmit Power	43 dbm	20 dbm
Antenna Gain	14dBi	0dBi
Antenna Type	120°	360°
Antenna back loss	20dB	–
Fast Fading	SCME	SCME
Shadowing Deviation	4 dB	4 dB
Penetration Loss	10dB	10dB
Noise Level	-174dBm/Hz	-174dBm/Hz
UE Distribution Density	$5 * 10^{-4}/m^2$	$1.4 * 10^{-3}/m^2$
Dynamic UE Rate	η_u=0.5	η_f=0.5

TABLE 2. Path Loss Model

Parameters	Value
MBS to MUE Path Loss	$131.1 + 42.8 * log_{10}\left(\frac{d_{m,B}}{1000}\right) + 20 * \delta_m$
FBS to FUE Path Loss	$127 + 30 * log_{10}\left(\frac{d_{j_f,f}}{1000}\right) + 20 * \left(1 - \delta_{j_f}\right)$
MBS to FUE Path Loss	$131.1 + 42.8 * log_{10}\left(\frac{d_{j_f,B}}{1000}\right) + 20 * \delta_{j_f}$
FBS to MUE Path Loss	$127 + 30 * log_{10}\left(\frac{d_{m,f}}{1000}\right) + 20 * (1 - \delta_m)$

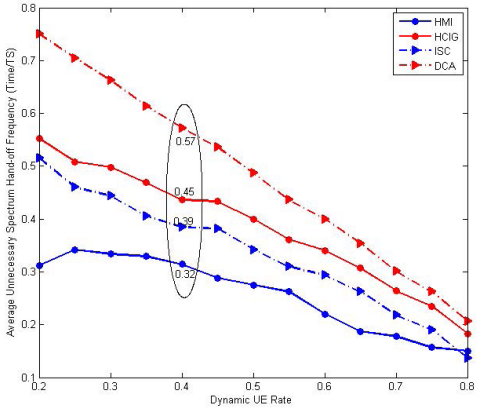

FIGURE 9. Average Subband Handoff frequency vs. dynamic UE ratio.

IV. SIMULATION RESULTS

In this section, the performance of the proposed FAS scheme is evaluated via simulation. The simulation parameters are listed in Table 1 by following 3GPP LTE specifications [24].

A 19 cell 57 sector cell configuration is used in the simulation. For a better accuracy on interference evaluation, simulation results are only collected from the center 7 cells [25]. MUEs are randomly distributed over the MC areas and FUEs are randomly distributed in the coverage area of FCs, both following PPP. The path loss model is introduced in Table 2 [26] and the fading follows a Rayleigh distribution. The path-loss from the BS (MBS or FBS) to an UE (MUE or FUE) depends on whether that UE is indoor or outdoor, which is captured by the indicator function. $\delta = 1$ is for indoor and $\delta = 0$ is for outdoor. And in the following simulations, we define the dynamic UE rate as: $\eta = \frac{n_{(m,t)}+n_{(f,t)}}{|\boldsymbol{M}|+|\boldsymbol{J_F}|}$.

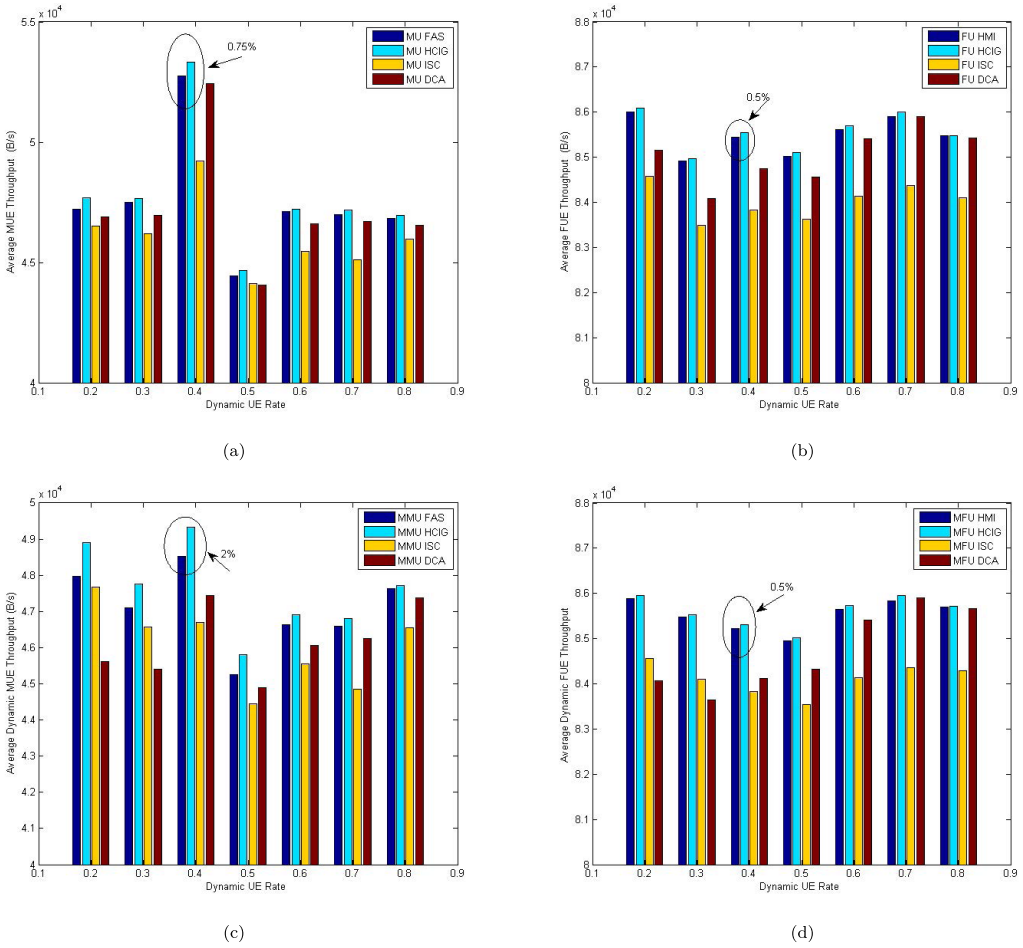

FIGURE 10. **Average throughput of UE vs. dynamic UE Rate. (a) Average MUE throughput. (b) Average FUE throughput. (c) Average dynamic MUE throughput. (d) Average dynamic FUE throughput.**

The performance of FAS scheme is compared with three other schemes, namely optimal heterogeneous cluster-based greedy scheme (OHCIG), interference-separation clustering-based scheme (ISC) [17], and multi-cluster based dynamic subband assignment (MC-DCA) [15]. As mentioned in Section III, the total computational complexity of the FAS scheme is $O((N^D)^2)$. OHCIG scheme is a common polling process. In every polling circle, N UEs join the polling process. So the computational complexity of OHCIG is $O((N)^2)$. Further, the computational complexity of ISC has been proved by the authors [17], which is $O((N)^2)$. The total computational complexity of MC-DCA scheme, which is also a common roll polling algorithm, is $O((N)^2)$ [15].

Fig. 8 shows the a Monte-Carlo experiment results of optimal ISM Similarity Factor threshold S_{th} for the FAS algorithm, where MU stands for all MUEs, FU stands for all FUEs, MMU stands for dynamic MUEs, and MFU stands for dynamic FUEs. As shown in Fig. 8.(a), when S_{th} increases, the average throughput of MUEs increases slowly and reaches a peak when $S_{th} = 0.6$. The average throughput of MMUs increases with the increase of S_{th} and achieves the biggest value when $S_{th} = 0.8$. Further, one can see

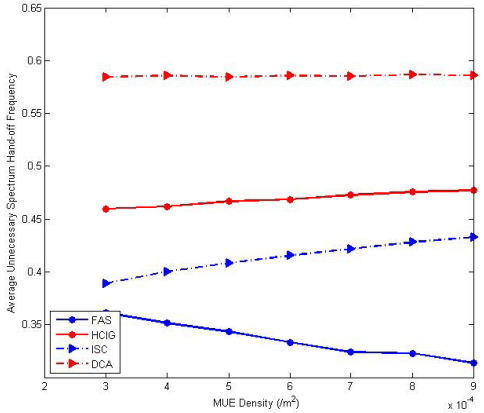

FIGURE 11. **Average Subband Handoff frequency with different MUE density.**

from Fig. 8.(b) that the average throughput of FUEs can reach two peaks at $S_{th} = 0.6$ and $S_{th} = 0.8$, respectively. Fig. 8.(c) shows the subband handoff time (NHT) of each UE averaged over 100 TSs. As S_{th} increases, NHT increases

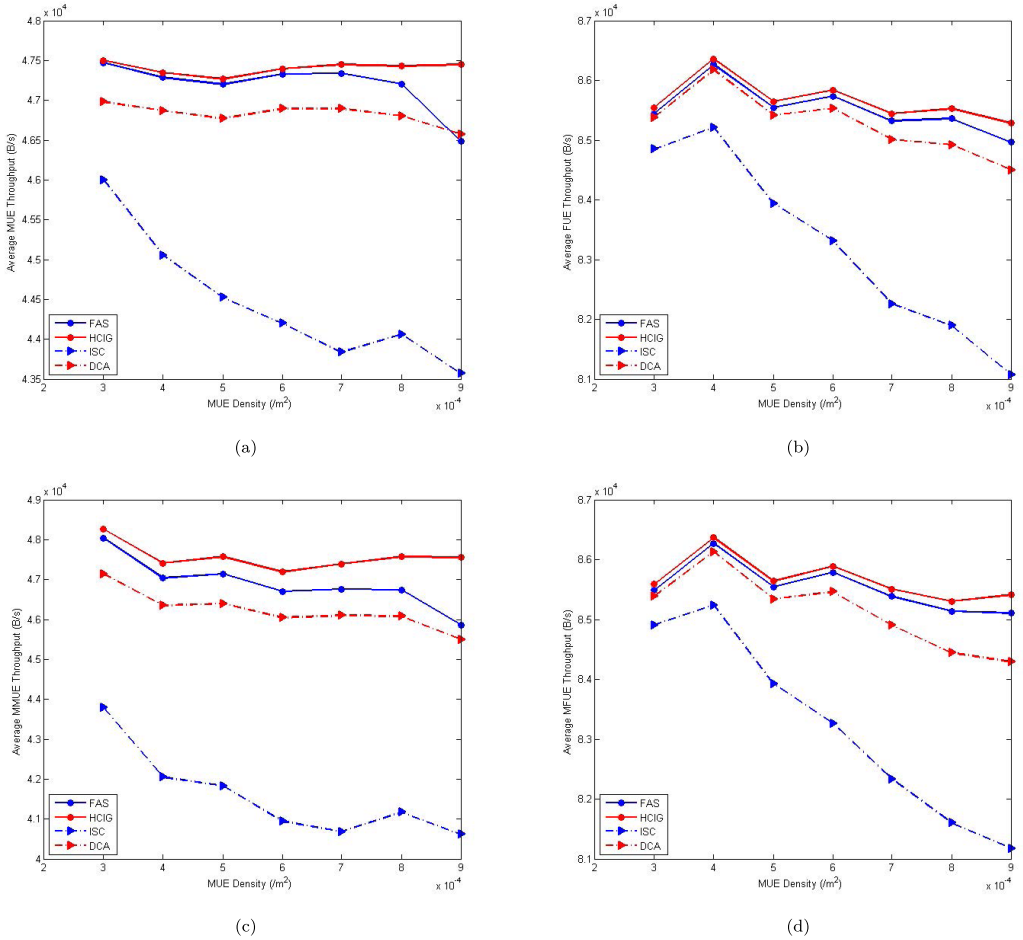

FIGURE 12. Average throughput of UE vs. MUE density. (a) Average MUE throughput. (b) Average FUE throughput. (c) Average dynamic MUE throughput. (d) Average dynamic FUE throughput.

sharply and the value is 22.30 when $S_{th} = 0.9$, which means on average a UE needs to switch its subband usage every 4 TSs. By taking both the average UE throughput and NHT into considerations, $S_{th} = 0.6$ is selected in the following simulation results.

Fig. 9 shows the average subband handoff frequency as a function of dynamic UE rates. Fig. 10 presents the average throughput of UEs with different dynamic UE rate. There are two constraints that can affect the average subband handoff frequency, the subband re-allocation in HMI and the number of static UEs in the entire network. Generally, as the increase of Dynamic UE rate, the static UE rate decreases. Since the average subband handoff frequency is a parameter that indicates the unnecessary subband switch frequency of static UEs, the value decreases with the increase of dynamic UE rate, which is also proved in Fig. 9. Further, we can see there is a peak when dynamic UE rate is 0.25. That is because when the ratio of dynamic UEs is relatively low, the subband re-allocation in HMI has a major influence on the performance of average subband handoff frequency. Though the re-allocation is not frequent, the influence is apparent, so there is an increase trend when dynamic UE rate is smaller

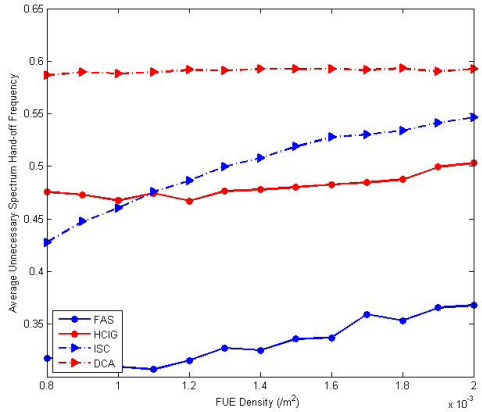

FIGURE 13. Average Subband Handoff frequency vs. FUE density.

than 0.3. Also, we can see that when the dynamic UE ratio varies, the performance of FAS scheme is better than the other three schemes. When the dynamic UE rate is 0.4, the average subband handoff frequency of FAS is 0.32, which is only 70% of the OHCIG scheme. And at the same time,

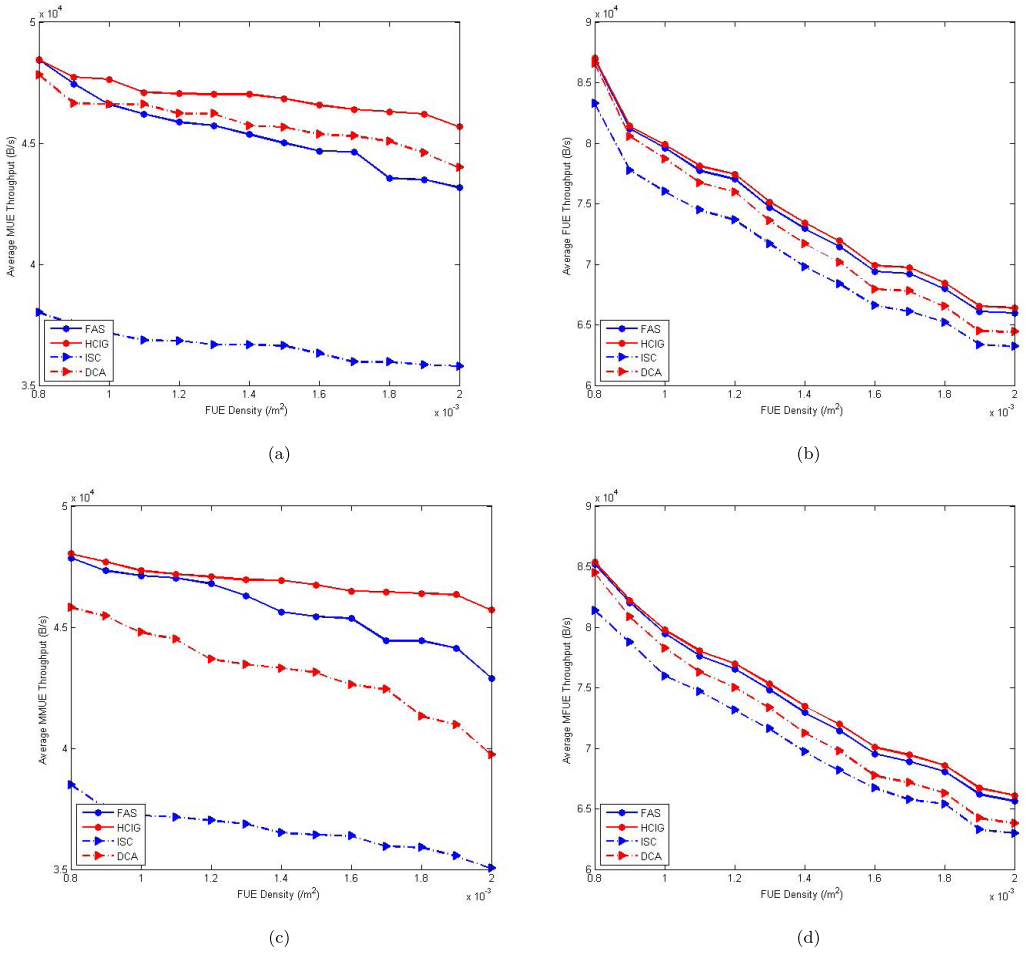

FIGURE 14. Average throughput of UE with different FUE density. (a) Average MUE throughput. (b) Average FUE throughput. (c) Average dynamic MUE throughput. (d) Average dynamic FUE throughput.

as shown in Fig. 10(a), the average MUE throughput of FAS scheme is only 0.75% worse than that of the OHCIG scheme and the average FUE throughput of FAS scheme is only 0.5% worse than that of the HCIG scheme. When it comes to the dynamic UEs, the biggest gap of average UE throughput between the FAS scheme and the OHCIG scheme appears when the dynamic UE rate is 0.4, which is 2% for MMUE and 0.5% for MFUE respectively.

Fig. 11 shows the average subband handoff frequency with different MUE densities. Fig. 12 shows the average UE throughput with different MUE Densities. From Fig. 11 we can see that, when the MUE density changes, the subband handoff restriction performance of the FAS scheme outperforms the other three schemes. When the MUE density is $6 * 10^{-4}$ per m^2, the subband handoff frequency of the FAS scheme is 0.33 per TS, which is 30% better than the OHCIG scheme, 19.5% better than ISC scheme and 42% better than the DCA scheme. As a marginal trade-off of this performance gain, as shown in Fig. 12, FAS has 0.2% MUE throughput decrease and 0.23% FUE throughput decrease compared with the OHCIG scheme. Dynamic MUE throughput shows the biggest difference among different schemes. There is an average 1.4% decrease in dynamic MUE throughput in the FAS scheme compared with the OHCIG scheme. When compared with the other two schemes, ISC scheme and DCA scheme, the FAS scheme presents an overall performance advantage on all categories.

Fig. 13 shows the average subband handoff frequency with different FUE densities. Fig. 14 shows the average throughput of UEs with different FUE Densities. From Fig. 13 we can see that, when the FUE density increases, the subband handoff frequency of all the schemes deteriorates. When more FUEs are located in the area under study, the more dynamics can occur in that area, which leads to a more frequent subband reallocation. In general, the FAS scheme outperforms the other three schemes. When the FUE density is $1.4 * 10^{-3}$ per m^2, the subband handoff frequency of FAS scheme is 0.325 per time slot, while the OHCIG scheme shows a value of 0.48 per time slot. The trade-off of this 32.3% improvement is 3.2% MUE average throughput degradation and 0.7% FUE average throughput degradation for FAS. When compared with the other two schemes, the FAS scheme has a lower MUE average

throughput performance than the DCA scheme but shows better performance on other categories.

V. CONCLUSIONS

In this paper, a fast subband allocation scheme is proposed to mitigate interference in an ultra dense dynamic heterogeneous network using cluster-based graph theory. In the existing interference mitigation schemes, UEs are normally assigned different subbands in different time slots, which leads to a high subband handoff rate and a high computational complexity. In this paper, a new subband allocation scheme allows static UEs to keep their allocated subbands when the network interference state meets certain conditions. Further, the proposed scheme is more efficient and offers a higher spectral efficiency than other frequency reuse schemes. The proposed FAS has a computational complexity $O((N^D)^2)$ and achieves almost the same spectral efficiency compared with the traditional UFR scheme, whose computational complexity $O(N^2)$ is much higher. The system level simulation show that the FAS has advantageous performance on subband handoff rate and latency while a reasonable trade-off on UE throughput is noted.

APPENDIX A

For the calculation of $h_m(i,j)$:

$$\begin{aligned} I_{\boldsymbol{M}}^{AAS} &= \frac{3\omega}{\pi\psi^2} + \frac{3\omega}{\pi\left((2\psi)^2-(\psi)^2\right)} + \cdots \\ &\quad + \frac{3\omega}{\pi\left(\left(n\psi\right)^2-\left(n-1\right)\psi\right)^2\Big)} \\ &= \frac{3\omega}{\pi\psi^2}\sum_{n=1}^{\Psi}\frac{1}{2n-1}, \end{aligned} \tag{36}$$

subject to:

$$\begin{cases} n = \lceil \dfrac{d}{\psi} \rceil, \\ \psi = \dfrac{2R}{\Psi}. \end{cases}$$

One can get:

$$\omega = \frac{\pi\psi^2 I_{\boldsymbol{M}}^{AAS}}{3\sum_{n=1}^{\Psi}\frac{1}{2n-1}}. \tag{37}$$

So we have

$$\begin{aligned} h_m(i,j) &= \frac{\omega}{\pi\left(2n-1\right)\psi^2 n_k} \\ &= \frac{\pi\psi^2 I_{\boldsymbol{M}}^{AAS}}{3\pi\left(2n-1\right)\psi^2 n_k\sum_{n=1}^{\Psi}\frac{1}{2n-1}} \\ &= \frac{I_{\boldsymbol{M}}^{AAS}}{3\left(2n-1\right)n_k\sum_{n=1}^{\Psi}\frac{1}{2n-1}}, \end{aligned} \tag{38}$$

where n_k is the total number of pixels whose distance d with the center point meets $(n-1)\,\psi < d \le n\psi$.

APPENDIX B

According to (19), we can get the limiting value of I_f^{AAS} whenwhen FBS f is within MBS's coverage area.

$$\begin{aligned} I_{f,max}^{AAS} &= \sum_{f^*\in\boldsymbol{F^*}}\frac{1}{1+2d_{f^*,f}^2\psi_{f^*}} + \sum_{m\in\boldsymbol{M}}\frac{P_f {d_{m,B}}^2}{P_B {d_{m,f}}^2}. \\ &\approx \frac{N_F-1}{1+2(\bar{d_{f^*,f}})^2\psi_{f^*}} + \frac{N_M P_f}{P_B}, \end{aligned} \tag{39}$$

$$N_F = |\boldsymbol{F}|, \tag{40}$$

$$N_M = |\boldsymbol{M}|, \tag{41}$$

$$\bar{d_{f^*,f}} = \frac{R_{min,f}\sum_{n_1=1}^{N_1}\sum_{n_2=1}^{N_2}\sqrt{(0.866n_2)^2+(n_1-1+0.5n_2)^2}}{N_F}, \tag{42}$$

subject to:

$$N_1 = \lceil\frac{R_\Delta}{R_{min,f}}\rceil, \tag{43}$$

$$\frac{N_2}{2} = \begin{cases} min\left(2n_1, \lceil\dfrac{R'}{R_{min,f}}\rceil\right), \\ \qquad\qquad n_1 \le \dfrac{R}{2R_{min,f}}; \\ min\left(-2n_1+4\lceil\dfrac{R}{2R_{min,f}}\rceil, \lceil\dfrac{R'}{R_{min,f}}\rceil\right), \\ \qquad\qquad n_1 > \dfrac{R}{2R_{min,f}}; \end{cases} \tag{44}$$

$$S_{min} = 0.866R_{min,f}^2, \tag{45}$$

$$N_F S_{min} = \frac{\pi}{3}R_\Delta^2, \tag{46}$$

$$\frac{2\sqrt{3}}{3}\sqrt{R_\Delta^2-(n_1R_{min})^2} = R'. \tag{47}$$

Then $h_{f,max}$ can be expressed as

$$h_{f,max} = \frac{I_{f,max}^{AAS}\psi^2}{S_{min}}. \tag{48}$$

According to (26), the limiting value of I_m^{AAS} is derived when FBS f is within MBS's coverage area.

$$I_{m,max}^{AAS} = \sum_{\substack{m^*,m\in\boldsymbol{M}\\ m^*\neq m}}\lambda_{m^*,m} + \sum_{f\in\boldsymbol{F}}\frac{P_B}{P_f\left(1+2d_{f,B}^2\psi_f\right)} \tag{49}$$

$$\approx N_M - 1 + \frac{N_F P_B}{P_f\left(1+2\bar{d_{f^*,f}}^2\psi_f\right)}, \tag{50}$$

and

$$I_{\boldsymbol{M},max}^{AAS} = N_M I_{m,max}^{AAS}. \tag{51}$$

Based on (28), $h_{m,max}$ can be found when $n=1$.

$$h_{m,max} = \frac{I_{\boldsymbol{M},max}^{AAS}}{3\sum_{n=1}^{\Psi}\frac{1}{2n-1}}. \tag{52}$$

Finally we have

$$ISM_{max} = h_{f,max} + h_{m,max}. \tag{53}$$

TABLE 3. Frequently Used Notations (Ordered by Appearance)

Notations	Meaning
R_M	MBS coverage radius
λ_m	MUE density
λ_f	FUE density
R_f	FBS coverage radius
$n_{(m,t)}$	MUE number in TS t
$n_{(f,t)}$	FUE number in TS t
P_{MBS}	MBS transmit power
P_{FBS}	FBS transmit power
k	Subband label
m	MUE label
n	MBS (or MC) label
f	FBS label
j_f	FUE j served by FBS f
$P_{B,m}^{k,t}$	Transmit power from MBS to MUE m on subband k in time slot t
$h_{B,m}^{k,t}$	Channel gain from MBS to MUE m on subband k in time slot t
$G_{B,m}^{k,t}$	Path loss from MBS to MUE m on subband k in time slot t
$P_{f,j_f}^{k,t}$	Transmit power from FBS f to FUE j on subband k in time slot t
$h_{f,j_f}^{k,t}$	Channel gain from FBS f to FUE j on subband k in time slot t
$G_{f,j_f}^{k,t}$	Path loss from FBS f to FUE j on subband k in time slot t
$\boldsymbol{M}$	The set of MUEs served by MBS
$s_m^{k,t}$	Subband allocation indicator
$\boldsymbol{F^*}$	The set of FBSs covered by MBS except f
$\boldsymbol{J_{f^*}}$	The set of FUEs served by FBS f^*
$\boldsymbol{F^*}$	The set of FBSs covered by MBS
$\boldsymbol{J_f}$	The set of FUEs served by FBS f
$\boldsymbol{K}$	The set of all available subbands
N_0	The noise level
$\boldsymbol{U}$	The set of all the UEs in the coverage area of MBS
$\boldsymbol{T}$	The total number of time slot in the whole test stage
$R_{min,f}$	The minimum between FBS and its serving FUE
$d_{f^*,f}$	The distance between FBS f^* and f
$d_{m,f}$	The distance between MUE m and FBS f
$\boldsymbol{\varpi}$	Antenna back loss
$\boldsymbol{\Theta_m}$	Sector label of MUE m
ψ	Pixel length; Minimum distance between two different UEs
$\boldsymbol{M_{S_0}}$	The set of MUEs locate at sector 0
$\boldsymbol{U_M^D}$	The set of dynamic MUEs
$\boldsymbol{U_F^D}$	The set of dynamic FUEs
η	Dynamic UE rate
η_m	Dynamic MUE rate
η_f	Dynamic FUE rate

APPENDIX C

See Table 3.

REFERENCES

[1] I. Hwang, B. Song, and S. S. Soliman, "A holistic view on hyper-dense heterogeneous and small cell networks," *IEEE Commun Mag.*, vol. 51, no. 6, pp. 20–27, Jun. 2013.

[2] J. G. Andrews *et al.*, "What will 5G be?" *IEEE J. Sel. Areas Commun.*, vol. 32, no. 6, pp. 1065–1082, Jun. 2014.

[3] H. Peng, Y. Xiao, Y. N. Ruyue, and Y. Yifei, "Ultra dense network: Challenges, enabling technologies and new trends," *China Commun.*, vol. 13, no. 2, pp. 30–40, Feb. 2016.

[4] *Small Cell Forum Calls Upon Telecoms Regulators to Enable Rapid Deployment of Dense HetNets for 5G*. (Oct. 2016). [Online]. Available: http://www.smallcellforum.org/

[5] S. Chen, F. Qin, B. Hu, X. Li, and Z. Chen, "User-centric ultra-dense networks for 5G: Challenges, methodologies, and directions," *IEEE Wireless Commun.*, vol. 23, no. 2, pp. 78–85, Feb. 2016.

[6] Y. Sui, I. Guvenc, and T. Svensson, "Interference management for moving networks in ultra-dense urban scenarios," *EURASIP J. Wireless Commun. Netw.*, vol. 1, no. 1, pp. 1–32, 2015.

[7] M.-C. Chuang, M. C. Chen, and S. Yeali, "Resource management issues in 5G ultra dense smallcell networks," in *Proc. IEEE ICOIN*, Cambodia, Asia, Jan. 2015, pp. 159–164.

[8] F. Mhiri, K. Sethom, and R. Bouallegue, "A survey on interference management techniques in femtocell self-organizing networks," *J. Netw. Comput. Appl.*, vol. 36, no. 1, pp. 58–65, 2013.

[9] Y. L. Lee, T. C. Chuah, J. Loo, and A. Vinel, "Recent advances in radio resource management for heterogeneous LTE/LTE-A networks," *IEEE Commun. Surveys Tuts.*, vol. 16, no. 4, pp. 2142–2180, 4th Quart., 2014.

[10] M. Peng, C. Wang, J. Li, H. Xiang, and V. Lau, "Recent advances in underlay heterogeneous networks: Interference control, resource allocation, and self-organization," *IEEE Commun. Surveys Tuts.*, vol. 17, no. 2, pp. 700–729, 2nd Quart., 2015.

[11] A. Abdelnasser and E. Hossain, "Subchannel and power allocation schemes for clustered femtocells in two-tier OFDMA hetnets," in *Proc. IEEE ICC*, Budapest, Hungary, Jun. 2013, pp. 1129–1133.

[12] O. Anjum, O. N. C. Yilmaz, C. Wijting, and M. A. Uusitalo, "Traffic-aware resource sharing in ultra-dense small cell networks," in *Proc. IEEE EuCNC*, Paris, France, Jul. 2015, pp. 195–199.

[13] A. R. Elsherif, W.-P. Chen, A. Ito, and Z. Ding, "Adaptive resource allocation for interference management in small cell networks," *IEEE Trans. Commun.*, vol. 63, no. 6, pp. 2107–2125, Jun. 2015.

[14] L. Zhou *et al.*, "A dynamic graph-based scheduling and interference coordination approach in heterogeneous cellular networks," *IEEE Trans. Veh. Technol.*, vol. 65, no. 5, pp. 3735–3748, May 2016.

[15] S.-J. Kim, I. Cho, B. Lee, S.-H. Bae, and C.-H. Cho, "Multi-cluster based dynamic channel assignment for dense femtocell networks," *Trans. Int. Inf. Syst.*, vol. 10, no. 4, pp. 1535–1554, Apr. 2016.

[16] M. Yoon, M.-S. Kim, and C. Lee, "A dynamic cell clustering algorithm for maximization of coordination gain in uplink coordinated system," *IEEE Trans. Veh. Technol.*, vol. 65, no. 3, pp. 1752–1760, Mar. 2016.

[17] J. Qiu, Q. Wu, Y. Xu, Y. Sun, and D. Wu, "Demand-aware resource allocation for ultra-dense small cell networks: An interference-separation clustering-based solution," *Trans. Emerg. Telecommun. Technol*, vol. 27, no. 8, pp. 1071–1086, 2016.

[18] Z. Zhang, R. Q. Hu, Y. Qian, A. Papathanassiou, and G. Wu, "D2D communication underlay uplink cellular network with fractional frequency reuse," in *Proc. IEEE DRCN*, Kansas City, KS, USA, May 2015, pp. 247–250.

[19] A. Gotsis, S. Stefanatos, and A. Alexiou, "UltraDense networks: The new wireless frontier for enabling 5G access," *IEEE Veh. Technol. Mag.*, vol. 11, no. 2, pp. 71–78, Feb. 2016.

[20] Y. Li, C. Niu, F. Ye, and R. Q. Hu, "A universal frequency reuse scheme in LTE-A heterogeneous networks," *Wireless Commun. Mobile Comput.*, vol. 16, no. 17, pp. 2839–2851, Sep. 2016.

[21] C. Niu, Y. Li, R. Q. Hu, and F. Ye, "A femtocell enhanced multi-target spectrum allocation strategy in LTE-A HetNets," *IET Commun.*, Dec. 2016.

[22] Z. Wang, A. C. Bovik, H. R. Sheikh, and E. P. Simoncelli, "Image quality assessment: From error visibility to structural similarity," *IEEE Trans. Image Process.*, vol. 13, no. 4, pp. 600–612, Apr. 2004.

[23] A. Hore and D. Ziou, "Image quality metrics: PSNR vs. SSIM," in *Proc. IEEE ICPR*, Istanbul, Turkey, Aug. 2010, pp. 2366–2369.

[24] *Evolved Universal Terrestrial Radio Access (E-UTRA); Radio Frequency (RF) System Scenarios*, document TR 36.942 V8.2.0, 3GPP, Jun. 2010. [Online]. Available: www.3gpp.org/ftp/Specs/

[25] R. Wei, Y. Wang, and Y. Zhang, "A two-stage cluster-based resource management scheme in ultra-dense networks," in *Proc. IEEE ICCC*, Shanghai, China, Oct. 2014, pp. 738–742.

[26] F. Pantisano, M. Bennis, W. Saad, M. Debbah, and M. Latva-Aho, "Interference alignment for cooperative femtocell networks: A game-theoretic approach," *IEEE Trans. Mobile Comput.*, vol. 12, no. 11, pp. 2233–2246, Nov. 2013.

CHONGYU NIU received the B.S. degree in electronical information from Harbin Engineering University in 2012. He is currently pursuing the P.D. degree in Harbin Engineering University with the Department of Information and Communication Engineering. His main studying area is interference mitigation and resource allocation in HetNets.

YIBING LI (M'09) received the B.S., M.S., and Ph.D. degrees from the Harbin Marine Engineering College, Harbin Engineering University, Heilongjiang, China, in 1989, 1997, and 2003, respectively. He has been a Teacher with the Harbin Engineering University of China since 1989, and became a Professor in 2004. From 2007 to 2008, he was with the Electronic Engineering Laboratory, The University of Hong Kong, as a Visiting Scholar. He is currently a Professor with the Department of Information and Communication Engineering, Harbin Engineering University. He is a Senior Member of the China Institute of Communications and the China Computer Federation.

ROSE QINGYANG HU received the B.S. degree in electrical engineering from the University of Science and Technology of China, the M.S. degree in mechanical engineering from the Polytechnic Institute of New York University, and the Ph.D. degree in electrical engineering from The University of Kansas. From 2002 to 2004, she was an Assistant Professor with the Department of Electrical and Computer Engineering, Mississippi State University. She also has over ten years of research and development experience with Nortel, RIM, and Intel as a Technical Manager, a Senior Wireless System Architect, and a Senior Research Scientist. She is currently an Associate Professor with the Department of Electrical and Computer Engineering, Utah State University. Her current research interests include next-generation wireless communications, wireless network design and optimization, green radios, multimedia QoS/QoE, communication and information security, and wireless system modeling and performance analysis. She has published extensively and holds numerous patents in her research areas. She is a member of Phi Kappa Phi and Epsilon Pi Epsilon Honor Societies. One of her co-authored papers received the Best Paper Award at the IEEE GLOBECOM 2012. She is currently serving on the editorial boards of the IEEE WIRELESS COMMUNICATIONS, the IEEE INTERNET OF THINGS JOURNAL, the IEEE COMMUNICATIONS TUTORIALS AND SURVEYS, the *Security and Communication Networks Journal*, *Wireless Communications and Mobile Computing*, and *KSII Transactions on Internet and Information Systems*. She has also been a six-time Guest Editor of the *IEEE Communications Magazine*, the IEEE WIRELESS COMMUNICATIONS, and the IEEE NETWORK.

FANG YE (M'09) received the B.S. and P.D. degrees in electrical information engineering from Harbin Engineering University (HEU), Heilongjiang, China, in 2002 and 2006, respectively. She has been a Teacher with the Harbin Engineering University of China since 2002, and became an Associate Professor in 2007. From 2007 to 2008, she was with the School of Electronics and Computer Science, University of Southampton, as a Visiting Scholar. She is currently an Associate Professor with the Department of Information and Communication Engineering, HEU. She is a member of the China Institute of Communications and the China Computer Federation.